Geochemistry Geophysics Geosystems G3
AN ELECTRONIC JOURNAL OF THE EARTH SCIENCES
Published by AGU and the Geochemical Society

Article
Volume 9, Number 12
5 December 2008
Q12008, doi:10.1029/2008GC002164
ISSN: 1525-2027

Lava lake surface characterization by thermal imaging: Erta 'Ale volcano (Ethiopia)

L. Spampinato
Istituto Nazionale di Geofisica e Vulcanologia, sezione di Catania, Piazza Roma 2, I-95123 Catania, Italy

Department of Geography, University of Cambridge, Downing Place, Cambridge, CB2 3EN, UK (spampinato-l@ct.ingv.it)

C. Oppenheimer
Department of Geography, University of Cambridge, Downing Place, Cambridge, CB2 3EN, UK

S. Calvari
Istituto Nazionale di Geofisica e Vulcanologia, sezione di Catania, Piazza Roma 2, I-95123 Catania, Italy

A. Cannata
Dipartimento di Scienze Geologiche, Università di Catania, Corso Italia 57, I-95129 Catania, Italy

P. Montalto
Dipartimento di Ingegneria Elettrica, Elettronica e dei Sistemi, Università di Catania, Viale A. Doria 6, I-95125 Catania, Italy

Istituto Nazionale di Geofisica e Vulcanologia, sezione di Catania, Piazza Roma 2, I-95123 Catania, Italy

[1] Active lava lakes represent the exposed, uppermost part of convecting magma systems and provide windows into the dynamics of magma transport and degassing. Erta 'Ale volcano located within the Danakil Depression in Ethiopia hosts one of the few permanent convecting lava lakes, probably active for a century or more. We report here on the main features of the lava lake surface based on observations from an infrared thermal camera made on 11 November 2006. Efficient magma circulation was reflected in the sustained transport of the surface, which was composed of pronounced incandescent cracks that separated wide plates of cooler crust. These crossed the lake from the upwelling to the downwelling margin with mean speeds ranging between 0.01 and 0.15 m s^{-1}. Hot spots eventually opened in the middle of crust plates and/or along cracks. These produced mild explosive activity lasting commonly between ~10 and ~200 s. Apparent temperatures of cracks ranged between ~700 and 1070°C, and of crust between ~300 and 500°C. Radiant power output of the lake varied between ~45 and 76 MW according to the superficial activity and continuous resurfacing of the lake. Time series analysis of the radiant power output data reveals cyclicity with a period of ~10 min. The combination of visual and thermal observations with apparent mean temperatures and convection rates allows us to interpret these signals as the periodic release of hot overpressured gas bubbles at the lake surface.

Components: 7529 words, 10 figures.

Keywords: Erta 'Ale; lava lake; thermal imaging; heat flux radiant power output.

Index Terms: 8485 Volcanology: Remote sensing of volcanoes; 3270 Mathematical Geophysics: Time series analysis (1872, 4277, 4475).

Received 9 July 2008; **Revised** 22 September 2008; **Accepted** 30 September 2008; **Published** 5 December 2008.

Spampinato, L., C. Oppenheimer, S. Calvari, A. Cannata, and P. Montalto (2008), Lava lake surface characterization by thermal imaging: Erta 'Ale volcano (Ethiopia), *Geochem. Geophys. Geosyst.*, *9*, Q12008, doi:10.1029/2008GC002164.

1. Introduction

[2] Active lava lakes represent the uppermost level of convection currents that stir molten, gas-rich, magmas within conduits [*Tilling*, 1987; *Tazieff*, 1994]. Conduit convection, driven most likely by density contrasts resulting from degassing, is the clearest conceptual model explaining the longevity of lava lakes [*Kazahaya et al.*, 1994; *Stevenson and Blake*, 1998; *Huppert and Hallworth*, 2007]. Heat lost from the lake surface is balanced by the enthalpy difference between magma ascending and sinking in the conduit [*Francis et al.*, 1993; *Harris et al.*, 1999; *Oppenheimer et al.*, 2004; *Harris et al.*, 2005]. It has been argued that the stability of lava lakes is strictly dependent on lake-conduit geometry, solubility and gas expansion, and magma volatile content [*Witham and Llewellin*, 2006].

[3] Persistent lava lakes are currently hosted at the summits of Erta 'Ale volcano (Ethiopia), Nyragongo volcano (Democratic Republic of Congo), and Mt. Erebus (Ross Island, Antarctica). Despite the differences in Erta 'Ale, Erebus, and Nyragongo magma compositions (tholeiitic basalt, anorthoclase phonolite, and nephelinite, respectively), *Tazieff* [1994] highlighted common surface features including superficial currents, hot spots, explosive activity, variations in lake level, variations of the lake surface speed, and convection to be common to the three lakes. Several authors have examined lava lake dynamics focusing on gas and thermal budgets, seismicity, description of surface features, and eruptive style at Erta 'Ale [e.g., *Le Guern et al.*, 1979; *Oppenheimer and Francis*, 1997, 1998; *Burgi et al.*, 2002; *Oppenheimer and Yirgu*, 2002; *Allard et al.*, 2004; *Oppenheimer et al.*, 2004; *Jones et al.*, 2006]. Erebus [e.g., *Calkins et al.*, 2008; *Sweeney et al.*, 2008] and Nyiragongo [*Sawyer et al.*, 2008a]. Others modeled the superficial features of lava lakes [*Karlstrom and Manga*, 2006] and pattern of the crust movements on lake surfaces [*Matson et al.*, 2006; *Howell and Lopes*, 2007].

[4] In this paper we provide a detailed description of Erta 'Ale lava lake activity using ground-based thermal imaging performed on 11 November 2006 using a compact infrared thermal camera. In particular, we aim to elucidate aspects of the dynamics of magma circulation at the surface and the thermal behavior of the lake with respect to temperature variations, lava lake surface motion, and radiative heat loss. Movie S1 in the auxiliary material[1] shows the dynamics of Erta 'Ale volcano active lava lake at the surface.

2. Erta 'Ale Lava Lake

[5] Erta 'Ale (613 m above seal level) is a basaltic shield volcano elongated NNW–SSE, located in the center of the Erta 'Ale range within the Danakil Depression in Ethiopia. The region undergoes crustal extension, which is reflected in the subdued topography of the volcanic range (Figure 1). The summit caldera of Erta 'Ale volcano (1600×700 m^2) hosts two pit craters (the northern and central pits, Figure 1), which have both contained lava lakes during the period of scientific observations [*Oppenheimer and Francis*, 1998]. Recently, the lake within the ~150-m-diameter central crater has been most prevalent, while the northern pit has been a site of persistent fumarolic activity within the crater and around its rim [*Global Volcanism Network*, 1992; *Oppenheimer et al.*, 2004] (Figure 1).

[6] Early accounts of activity at the volcano were recorded by European explorers including *Munzinger* [1869], *Hildebrandt* [1875], and *Thesiger* [1996]. Their descriptions suggest that the volcano has been the site of magmatic activity for at least a century [*Oppenheimer and Francis*, 1997]. However, the harsh desert environment and Ethiopia's political situation from the mid-1970s to early 1990s have deterred continuous ground-based surveillance of the volcano. After sporadic field campaigns of the 1960s and early 1970s, scientific observations were achieved mostly by satellite imagery [e.g., *Oppenheimer and Francis*, 1997; *Harris et al.*, 1999].

[7] Since early 2001, more frequent ground-based and aerial surveys have been carried out [*Burgi et al.*,

[1] Auxiliary materials are available in the HTML. doi:10.1029/2008GC002164.

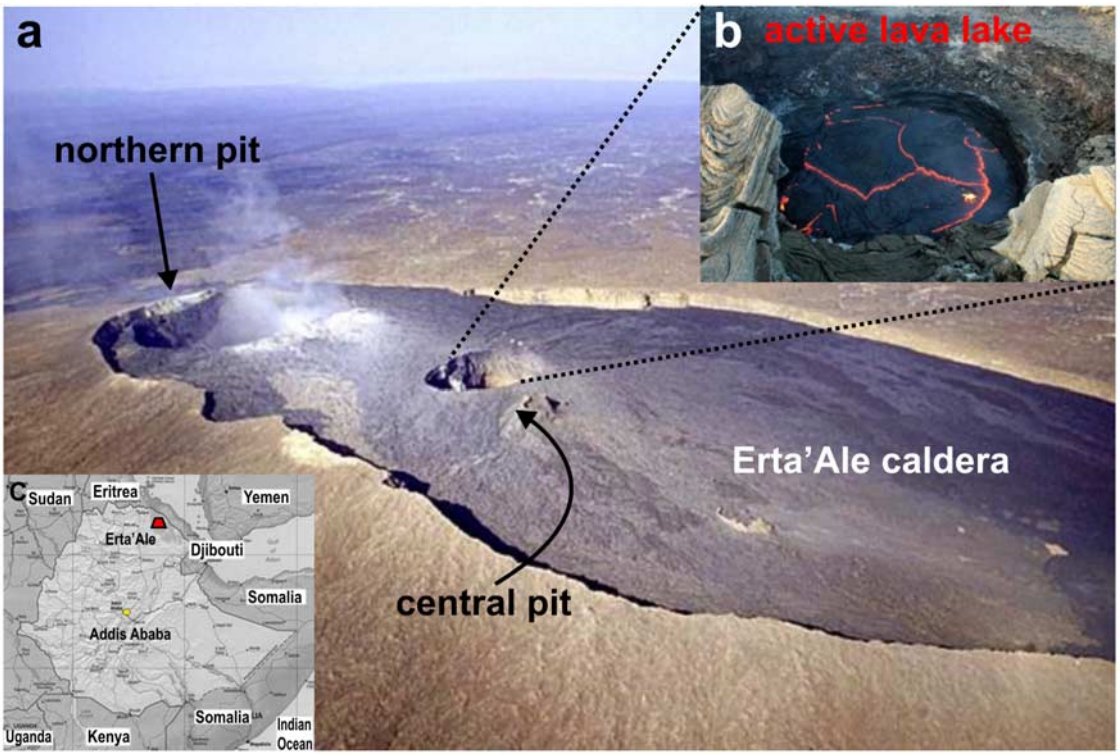

Figure 1. (a) Aerial photo taken from south of the summit area of Erta 'Ale volcano (Ethiopia) in February 2002 (courtesy of Jürg Alean, http://www.volcano.si.edu) with the elliptical caldera and the northern and central pits. The northern pit is characterized by degassing activity. (b) Aerial photo of the active lava lake within the central pit (http://danakil.ethiopia.free.fr). (c) Map of Ethiopia indicating the geographic location of Erta 'Ale volcano.

2002; *Oppenheimer and Yirgu*, 2002; *Oppenheimer et al.*, 2004; *Harris et al.*, 2005; *Jones et al.*, 2006]. These allowed better characterization of the lake surface activity and the assessment and modeling of eruptive dynamics.

[8] Important features of eruptive activity of Erta 'Ale include continuous magma convection and marked fluctuations of the lake level within the pit craters and changes in thermal characteristics, heat flux density, and area of the exposed surface as reported by several authors [*Barberi et al.*, 1973; *Tazieff*, 1973; *Le Guern et al.*, 1979; *Oppenheimer and Francis*, 1997; *Oppenheimer et al.*, 2004]. These studies reported opening of incandescent cracks; migration of thin, grayish, glassy crust plates from the lake's upwelling margin to the downwelling zone; and mild explosive activity. *Oppenheimer and Francis* [1997] discriminated between short- (minutes to hours) and long-term (tens to hundreds of days) variations in lake height due to degassing cycles and new magma input, respectively.

[9] Rare overspills also occurred, with lava spreading within the summit caldera and eventually flowing for a short distance down the volcano's flanks. Although such effusive episodes were rare, they provided valuable insights into the geometry of the shallow feeding system and conduits, as during the effusive activity that took place between 1968 and 1973. In that case, the simultaneous lava output at both pits was preceded by the lava level rising ~160 m in both pits, indicating their likely connection to a single deeper reservoir [*Oppenheimer and Francis*, 1997]. Concurrent with the geodynamic setting of the area, the low frequency of effusive eruptions (beyond the lava lake pits) suggests that the volcano growth is mainly due to endogenous processes (magmatic intrusion) as suggested by *Francis et al.* [1993] and *Oppenheimer and Francis* [1997].

3. Methods

[10] On 11 November 2006, Erta 'Ale lava lake data were recorded using an infrared thermal imager. The instrument was a P65 thermal camera manufactured by FLIR (Forward Looking Infra-Red) Systems. It consists of a 320 × 240 pixel uncooled-microbolometer-detector array sensitive across the 7.5–13 μm wave band and a corresponding 24 × 18° field of view (FOV). It

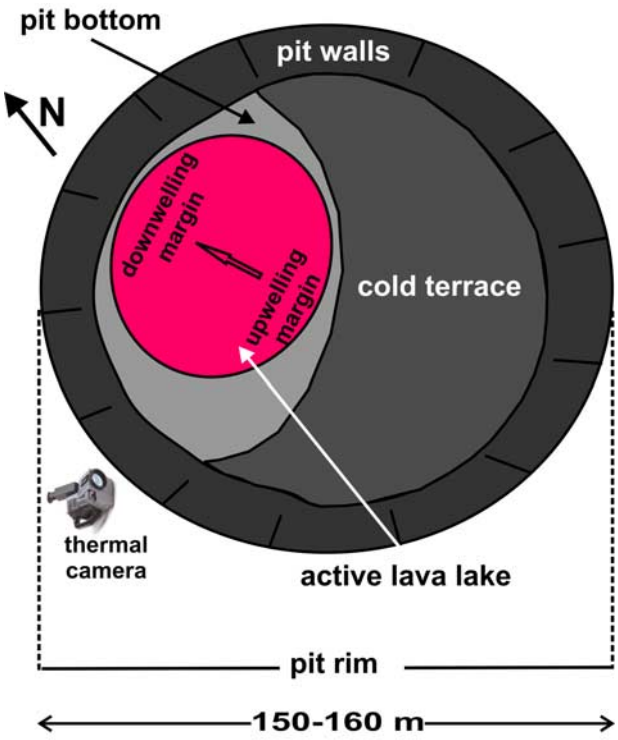

Figure 2. Sketch map of Erta 'Ale's central pit showing the location of the convecting, active lava lake (in red), zones of upwelling and downwelling, and the main direction of lava motion (black arrow). The site on the SW rim of the pit, from which thermal measurements were carried out on 11 November 2006, is shown.

has a thermal sensitivity of 0.08°C at 30°C and a quoted precision of ±2°C. The camera has three ranges of temperature measurement: −40 to 120°C, 0 to 500°C, and 350 to 1500°C.

[11] More than 3000 images and a thermal IR video were taken from the rim of Erta 'Ale central pit using the highest temperature range (Figure 2). The camera was tripod-mounted at an estimated distance of ∼70 m from the lava lake surface corresponding to a target pixel size of ∼0.1 m. Images were taken with a 6 s time step and captured about a third of the lava lake surface.

[12] To make a first-order atmospheric correction of the apparent temperatures, air temperature, relative humidity, and path lengths were input into the camera modeling software. However, we calculated brightness temperatures (i.e., for an emissivity of 1) to allow direct comparison with previous thermal studies [e.g., *Oppenheimer and Yirgu*, 2002; *Oppenheimer et al.*, 2004; *Harris et al.*, 2005]. Furthermore, in the absence of specific data on Erta 'Ale lava spectral emissivity, assuming an in-band emissivity for the hot basalt would not improve estimates of the radiative heat flux (the selected value would cancel out in the Stefan-Boltzmann equation).

[13] Then, we considered errors yielded by the oblique line-of-sight to the lake surface. On the basis of the thermal image size and lava lake dimensions, we estimated a viewing angle of ∼50° from the horizontal (maximum horizontal distance from the camera). According to *Ball and Pinkerton* [2006], for angles in between 0 (horizontal) and 60° the associated error varies up to 15%. This decreases the retrieved apparent temperatures (∼10°C) and thus lowers the radiant heat fluxes.

[14] However, in the absence of detailed geometrical control on our data set we have ignored these sources of error since they will have a very limited effect on characteristics of the radiative heat output time series.

[15] Surface speeds were estimated from the time taken for persistent features to cross the image field-of-view. Oblique viewing produces image distortion, thus variations of the pixel size according to the viewing angle and the path length. If the angle remains constant (∼50°), as in our case, pixels deform depending just on the distance. Using the dimension of the thermal image (320 × 240) and the size of the lava lake and the crater, we derived geometrically the minimum and maximum path length corresponding to the midpoints of the near and far margins of the image with respect to the camera. This allowed us to estimate the minimum and maximum pixel size, and considering the image size, the minimum and maximum distance crossed by the lava lake features. We estimated a distance uncertainty of ∼4% respect to the mean distance corresponding to ∼0.1 pixel size and ∼70 m path length.

[16] Photographs were contemporaneously collected using a Nikon D80 camera.

4. Erta 'Ale Lava Lake in November 2006: Surface Movements, Lava Lake Features, and Surface Eruptive Style

[17] The qualitative observations gained through the analysis of thermal and visible images of the vent area and lake center allowed characterization of the main features of the lava lake surface. On 11 November 2006, the lava lake consisted of wide crusted areas (crust plates) delineated by hot cracks and exhibited continuous resurfacing. The lava

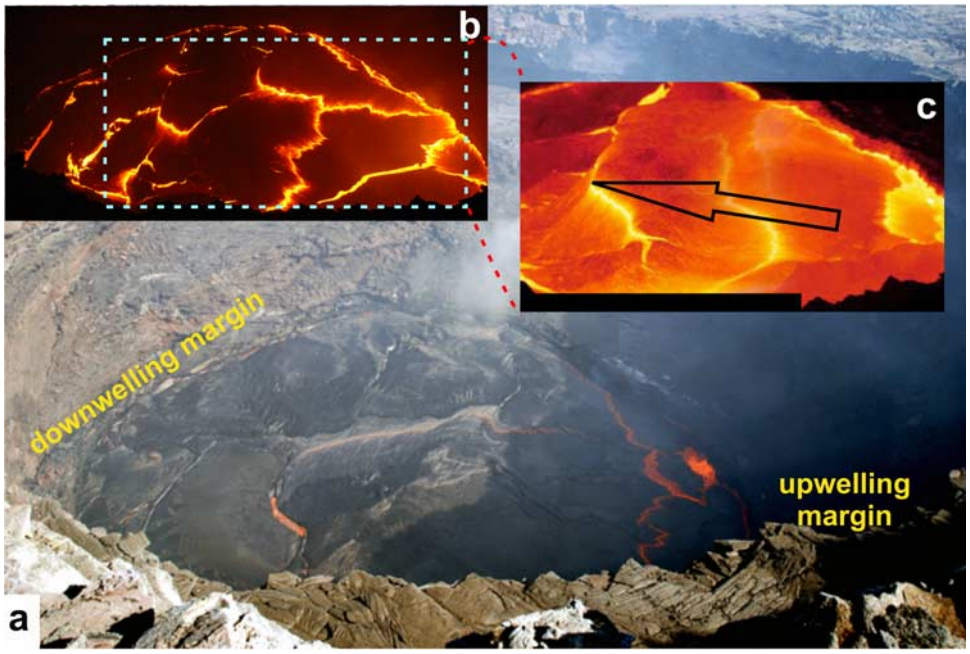

Figure 3. (a) Photo of Erta 'Ale lava lake taken from SW showing the lake surface appearance on 11 November 2006. (b) Photo of the lake taken from the same site in the evening of the same day. (c) Collage of two thermal images of the area corresponding to the dashed rectangle in Figure 3b; the black arrow indicates the main direction of surface motion.

lake surface spread from south to north, being fed from the southern edge of the lake and sinking at the opposite border (Figure 3).

[18] The source region of magma upwelling was quite broad and magma ascent generated surface waves with lava rapidly developing a grayish, glassy, chilled skin (Figure 4b, inset) rather than confined flows. Each wave was physically distinguished by marked alignments consisting of incandescent cracks developing almost parallel to the main spreading axis of the lake surface, as soon as the crust formed (Figures 3 and 4). These were characterized by the remarkable zigzag pattern thought to arise from the interaction between lava cooling and crust deformation, as modeled by *Karlstrom and Manga* [2006]. This is reminiscent of, at vastly different scale, transform faults at rifts that arise due to the differential velocity of spreading, magma output rates and stresses applied to the cooling lava.

[19] Chronologically, each "magma wave" showed an age-related crust temperature [*Turcotte and Schubert*, 2002] due to the "accretion" of new crust at the crack margins. As the crust ages with distance from the upwelling edge it cools and thickens [*Harris*, 2008]. Crust formed and deformed rapidly producing textures similar to Hawaiian ropey or pahoehoe lavas. These gave the magma waves lobate vertical profiles (a few centimeters in height, higher at the leading edge) with elongated tails, surmounted by relatively cool crust and outlined by glowing cracks (Figures 4a, 4b, and 4c). Lobes were likely the result of interaction between inflation and transport of magma below the surface, lava yield strength and flow resistance resulting from the crust (Figure 4b, inset). As shown in Figure 4b, radial growth of the crust was constantly fed by magma spreading at cracks. This typical development is clear from multiple parallel sutures visible on the crust surface, curved according to the main magma spreading direction (Figure 4b). Thus they provide indications on a lobe's age as shown in Figure 4b.

[20] As soon as crust developed and thickened, another class of cracks opened (Figure 4d) triggered by the stresses applied in order to accommodate the differential plate movements or due to the impingement of hot spots. These extended and widened, orthogonally to the lake-spreading axis, dividing the crust into further plates. As in the case of the main cracks, they also showed a zigzag pattern of margins. In periods of moderate/reduced activity, cracks cooled and closed forming wider compacted plates (Figure 5a).

[21] During the period of observation, the surface activity did not exhibit any pronounced variations in eruptive style; though surface motion varied

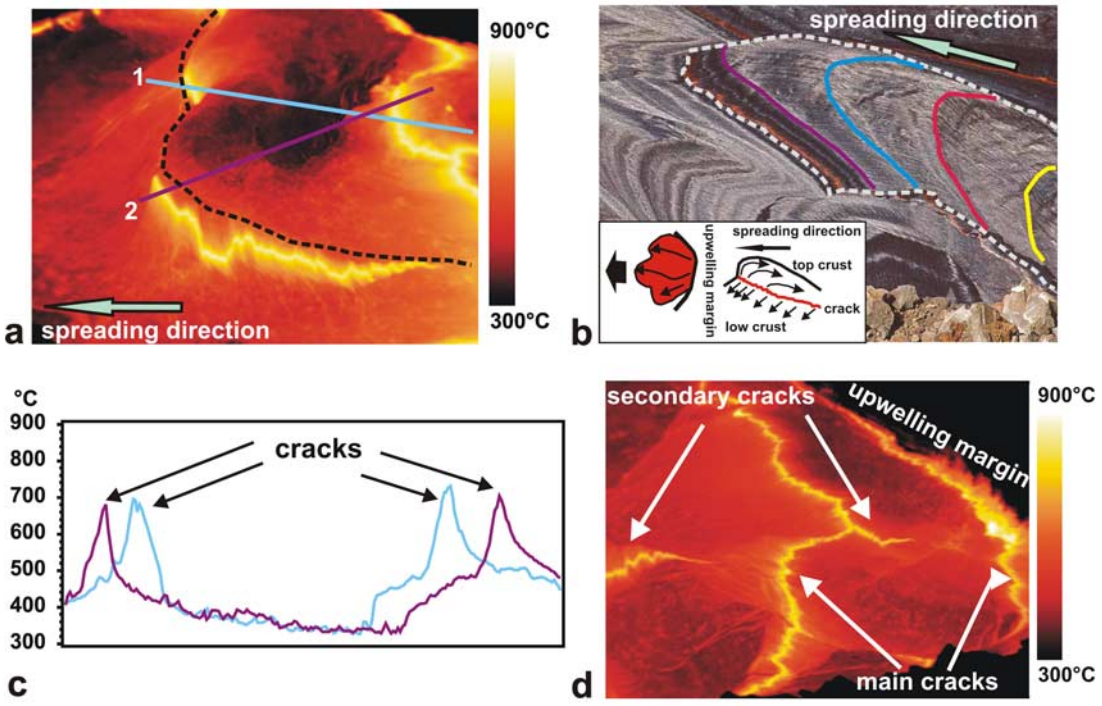

Figure 4. (a) Thermal image of the center of Erta 'Ale lava lake showing a distinct vertically lobate (black dashed line) lava surface wave. The region is delimited at the front and back by two incandescent cracks. (b) Photograph courtesy of Jürg Alean from http://www.swisseduc.ch taken in February 2002, showing a lobate lava wave (indicated by the white dashed line) and the main phases of crust growth (colored lines: purple line indicates the youngest portion of crust and yellow indicates the oldest). The inset is a sketch of lava wave propagation from the upwelling margin; plan and cross-sectional views. The profile highlights the vectors of crust propagation (curved arrows) that are opposite to the main direction of lake movement. (c) Two examples of thermal profiles of lava waves indicated in Figure 4a. In thermal profiles, lava lobe temperatures are substantially lower than the crack temperatures (apparent as peaks). (d) Thermal images of the upwelling area showing two classes of cracks (main and secondary cracks). The main cracks are the first to open parallel to the principal axis of the lake spreading. The secondary cracks form successively to accommodate the plate motion. In both cases it is possible to recognize the zigzag pattern described by *Karlstrom and Manga* [2006].

considerably from a low mean surface speed of $\sim$0.01 m s^{-1} (Figure 5a) up to a high mean of $\sim$0.15 m s^{-1} (Figure 5b) which was accompanied by mild explosive activity. In the more mobile stage, the more rapid and multidirectional motion disturbed the lake surface resulting in crust folding, a greater number of cracks, and crust collision (Figure 5b). This behavior was also accompanied by the opening of hot spots (Figure 5b). These consisted of small vents within plates ("intraplate spots" using the terminology of *Harris et al.* [2005]) or at crack intersections and developed at

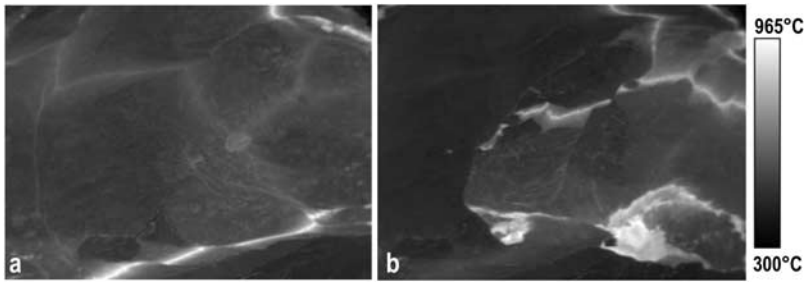

Figure 5. (a and b) Thermal images show the evolution of the same portion of the lake within 4.26 min. In Figure 5a the lake is characterized by moderate activity with cooling and coalescence of crust plates; in Figure 5b, during intense activity, hot spots develop emitting hot gases and lava, and a greater number of cracks open.

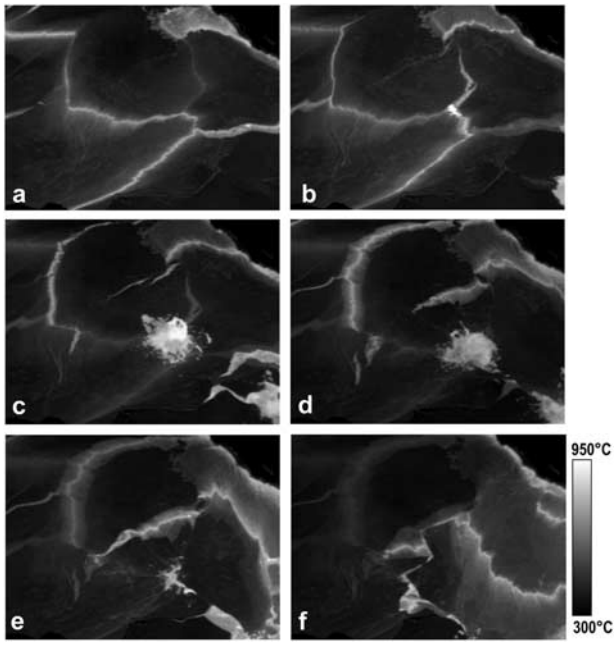

Figure 6. (a–f) Sequence of thermal images showing the activity of a hot spot and engulfment of the surrounding crust through time. This resulted in local change of the direction of lava motion.

a rate of ~8–12 per hour (Figure 5). They typically displayed bursts of ephemeral, overpressured gas bubbles at the surface and spattering activity lasting between ~10 and 200 s. This mild explosive activity yielded a sheet-like morphology to the lavas, which deformed rapidly acquiring the typical ropey-morphology of pahoehoe lava flows.

[22] Crust collision and hot spot opening usually triggered local variations in the lava spreading direction; in particular, the crust surrounding hot spots fractured and was engulfed with an almost whirling motion (Figure 6). The sinking of the crust around hot spots locally changed the direction of motion.

[23] Small variations in the lake level (~0.5–1 m) were also observed locally in areas close to the upwelling margin. However, we were unable to verify if these variations extended across the whole lake surface.

5. Quantitative Analysis of Thermal Imagery

[24] The infrared imaging of Erta 'Ale enabled tracking of the superficial thermal pattern of the active lava lake in terms of apparent temperature variations, frequency of temperature spatial distributions, and radiant power output.

5.1. Apparent Temperatures and Mean Cooling Rates

[25] From thermal images we retrieved apparent temperatures for either the upwelling area or the center of the lake (depending on pointing direction of the camera). Maximum apparent temperatures, obtained from each image, range between ~800 and 1020°C (from 1034:35 to 1133:33 UT) at the upwelling zone, and between ~750 and 1070°C (from 1500:56 and 1801:00 UT) in the lake center (Figure 7). Note that the peaks recorded at the lake center reach somewhat higher values (e.g., 1045, 1063, 1068, and 1070°C) than those measured at the upwelling margin (e.g., 1016, 1017, and 1020°C) and correspond commonly to burst of hot gas bubbles and/or to hot spots.

[26] Mean apparent temperatures recorded varied from ~450 to 540°C and ~400 to 500°C at the upwelling and central regions of the lake, respectively (Figure 7). Smoothing of the data (in Figure 7) highlights different trends. In particular, maximum apparent temperatures are characterized by narrow higher peaks and greater variability, whereas mean temperatures show a more regular sinusoidal trend on which a number of distinct and marked fluctuations are superimposed. Occasionally, these trends are in the opposite sense to the maximum apparent temperatures.

[27] The crust was typically between 300 and 500°C as shown in Figure 8. Here, a representative thermal image is shown with two-temperature contrast stretches to emphasize the distribution of incandescent cracks and crust.

[28] At the upwelling zone, new crust formed rapidly with mean estimated cooling rates of ~3.0°C s^{-1} and peaks of ~7.0°C s^{-1}, whereas in the middle of the lake, lava erupted from hot spots typically cooled at a rate of ~2.5°C s^{-1} with maximum rates of ~4.0°C s^{-1}.

5.2. Frequency of Temperature Spatial Distributions

[29] To investigate the thermal behavior of the lake and evolution of the surface dynamics, we looked at the frequency distribution of surface temperature (Figure 9). Figures 9a and 9b are two frequency distribution plots representative of the upwelling area of the lava lake (toward its southern margin), whereas Figures 9d and 9d represent the lake center. The four plots were selected according to the minimum (Figures 9a and 9c) and maximum mean temperature (Figures 9b and 9d) displayed

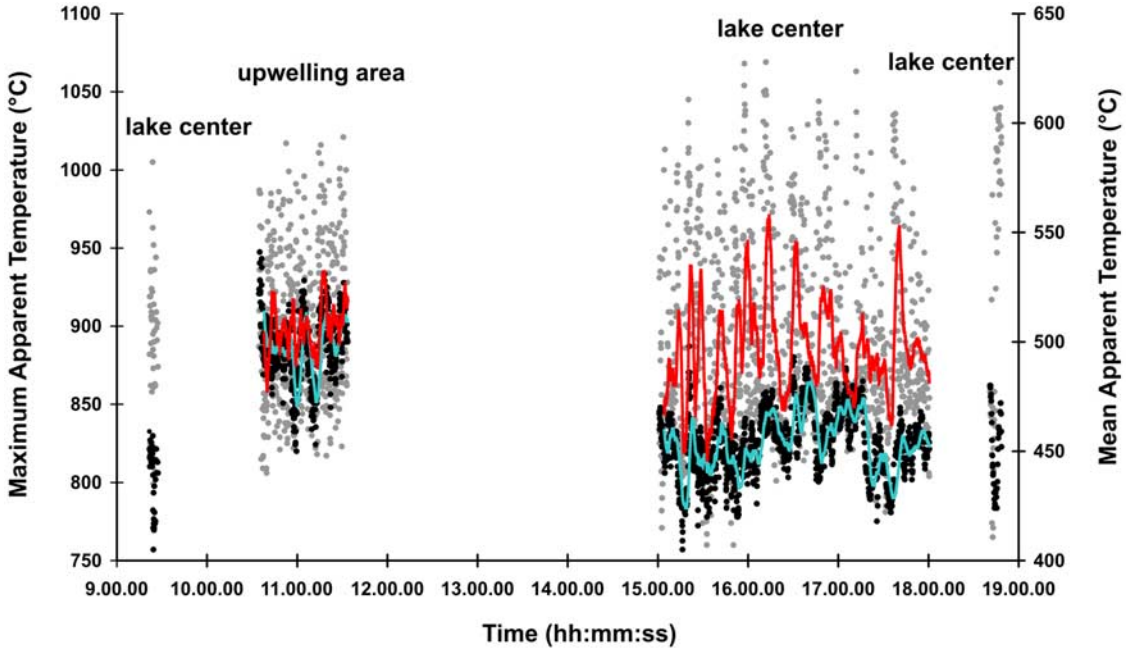

Figure 7. Graph showing the variability of maximum and mean apparent temperatures (gray and black dots, respectively) retrieved from the four sets of thermal images collected on 11 November 2006. The red and cyan lines are the corresponding 30-point running means. The first, third, and fourth data sets represent the lake center, whereas the second covers the upwelling zone at the southern margin of the lake. Measurements are affected by an uncertainty up to 15% due to the oblique viewing [*Ball and Pinkerton*, 2006].

by the upwelling and central areas of the lake, respectively.

[30] In the four histograms, the skewed distributions show elongated tails toward the highest temperatures (positive skewnesses, γ = 4.5, 4.3, 6.6, and 3.8 for Figures 9a, 9b, 9c, and 9d, respectively) consistent with the high contrast between crust and incandescent crack temperatures. Temperatures are asymmetrically clustered around the mean values (450, 540, 404, and 497°C for Figures 9a, 9b, 9c, and 9d, respectively) declining quite gradually (except for Figure 9b) toward the higher temperatures. The high standard deviations (σ = 100, 125, 61 and 29°C for Figures 9a, 9b, 9c, and 9d, respectively) indicate high statistical dispersion with the majority of temperatures far from the arithmetic mean.

[31] Figures 9a, 9c, and 9d show unimodal distributions with dominant mode between 350 and 400°C (Figures 9a and 9c) and between 350 and 450°C (Figure 9d). Figure 9b displays bimodal distributions with the highest frequencies occurring between 420 and 480°C (the dominant) and 790 and 840°C.

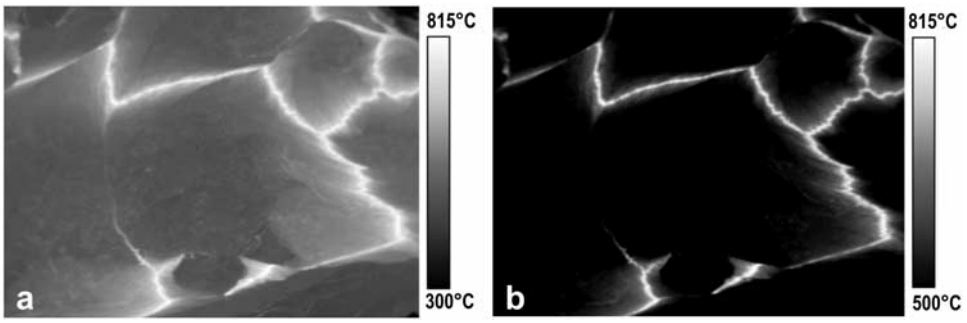

Figure 8. (a and b) The same thermal image collected in the center of Erta 'Ale lava lake on 11 November 2006. In Figure 8a the lower temperature threshold is 300°C, whereas in Figure 8b it is 500°C. Note that the crust temperature did not exceed 500°C.

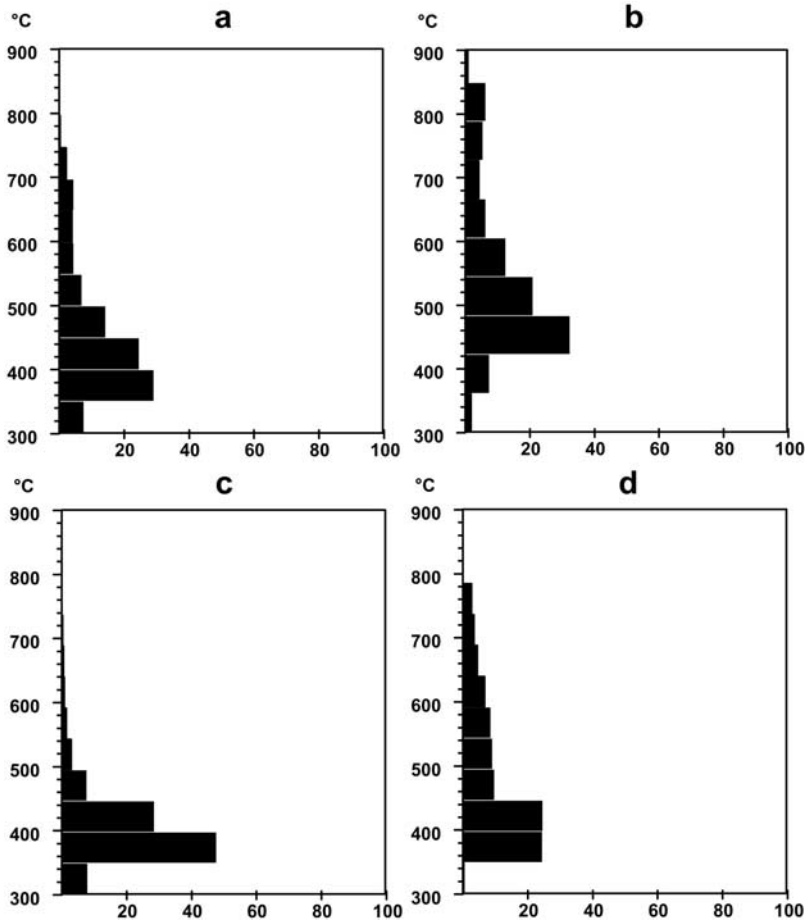

Figure 9. (a and b) Temperature frequency distributions for two thermal images covering at the upwelling zone on 11 November 2006 (1059:37 and 1035:03 UT); Figure 9a is characterized by low mean temperature and Figure 9b is characterized by a high mean value. (c and d) Images of the lake center for low and high mean temperatures, respectively (1516:20 and 1520:52 UT).

5.3. Radiant Power Output

[32] Owing to the thermal camera's FOV and viewing geometry, it was not possible to image the whole lava lake surface; however, we extrapolated the radiant power output (in MW) of the entire lake based on the estimate that the FOV corresponds to approximately a third of the total lake area and that the thermal distributions within the FOV are reasonably representative of the whole lake surface. Given the nature of these assumptions it is not possible to put robust constraints on the error budgets for the calculations so we consider the results as rough approximations and focus more on the analysis of time series of data.

[33] For radiant power output (Q_{rad}) calculations, we applied the Stefan-Boltzmann equation (1) to the lake surface temperature spatial distributions:

$$Q_{rad} = A\ \sigma\left(\Sigma f_i\ T_i^4\right) \qquad (1)$$

where A is the surface area of the lake, σ is the Stefan-Boltzmann constant, and f_i is the fractional area of material at a brightness temperature of T_i (note emissivity does not therefore appear in the equation). The quantity $\{\sqrt[4]{(\Sigma f_i T_i^4)}\}$ represents the effective radiation temperature (T_e).

[34] From visual observations we estimate that the active lake was roughly elliptical with major and minor axes of ~80 m and ~40 m, respectively, equivalent to an area of ~2500 m^2 (the same size of the major axis was observed between 26 December 2005 and 3 January 2006, http://www.volcano.si.edu/world/volcano.cfm). The total field of view of the image was estimated considering the pixel size for a mean 70 m line of sight. This yielded to an imaged area of the lake of ~730 m^2, which, compared with the third of the total lake area estimated empirically, gives an underestimate of ~100 m^2, likely due to the oblique viewing of the lake surface. Because of distortion of the area

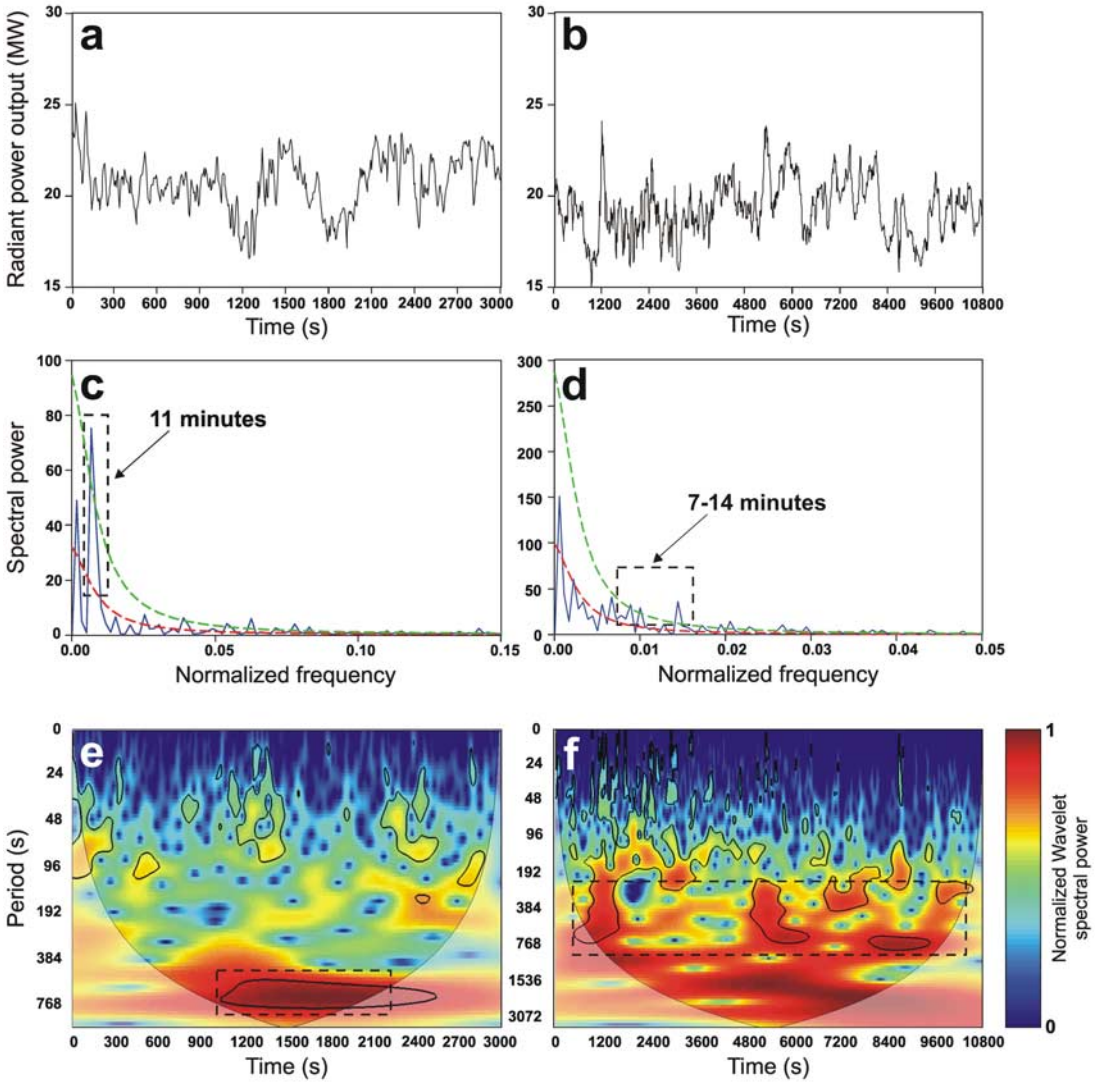

Figure 10. (a and b) Time series of the radiant power output (MW) retrieved for the second and third data sets shown in Figure 7, corresponding to the lake margin (upwelling zone) and center, respectively; (c and d) power spectra computed via periodogram normalized by standard deviation of the time series shown in Figures 10a and 10b. The red lower and the green upper dashed lines show estimated red noise spectrum and 95% confidence spectrum. (e and f) Wavelet transform, computed using a Matlab code provided by *Grinsted et al.* [2004], of the two time series. The solid contour shows the 95% confidence interval and the light shade shows the "cone of influence," the region where the wavelet spectrum is subject to edge effects [*Torrence and Compo*, 1998]. The dashed rectangles indicate the most significant periods.

imaged, we preferred to use the area estimated from direct observations in our calculations.

[35] Figures 10a and 10b show the radiant power output retrieved from the longest data sets presented in Figure 7. For both time series, Q_{rad} ranges between ~15 and 25 MW with mean values ~19 MW. Of the two data sets, the first indicates slightly higher values (~16–25 MW compared with ~15–24 MW). These measurements should be multiplied by 3 to provide estimates of the total radiated power from the lake surface.

[36] Inspection of the two time series suggests superimposition of both low- and high-frequency components. To investigate further, we used a wavelets-based time series analysis.

[37] In time series analysis we can represent information in two basic ways: time and frequency representations. The former does not display spectral content while the latter shows only frequency information. Frequency representation is commonly computed using the Fourier transform that allows the retrieval of information on power content at any

frequency. The widely used Fourier transform is designed for stationary signals; in classical Fourier analysis we lose the frequency location in the time domain. For the analysis of time series containing non-stationary power at many different frequencies, Short time Fourier transform (STFT) and wavelet transform (WT) are commonly applied [*Daubechies*, 1990]. In contrast to the Fourier transform, which consists of a linear superposition of independent and nonevolving periodicities, the WT is based on the convolution of signals with a set of functions derived from the translations and dilatations of a basic function called the "mother wavelet." In order to investigate the time variation of the spectral content of the thermal signals, WT was chosen rather than STFT. In fact, unlike STFT, WT gives a more accurate time-frequency description of signals containing low and high frequency components (as observed in the investigated signals in Figures 10a and 10b). Taking into account STFT method, once the length of the moving window is chosen, also the frequency resolution is fixed, and the entire phase space is uniformly described by cells of fixed sizes. Conversely, WT method, based on variable-sized cells, allows the use of long time intervals to gather more precisely low-frequency information, and of shorter regions for high-frequency information [*Bartosch and Seidl*, 1999; *Lesage et al.*, 2002]. Moreover, the use of the WT allows the study of periods comparable to the signal length.

[38] As argued by *Torrence and Compo* [1998], for many geophysical phenomena an appropriate background noise spectrum is either white or red noise. White noise is characterized by a flat Fourier spectrum, whereas red noise shows decreasing power with increasing frequency. Commonly, power spectra of geophysical time series are characterized by increasing power at lower frequencies and show many distinctive red noise features. Accordingly, peaks in the time series power spectrum are assumed significant if they exceed the 95% confidence spectrum computed based on the hypothesis of white or red background noise. Thus to investigate the most energetic periods contained in both our radiant power output time series shown in Figures 10a and 10b, the classical Fourier transform (Figures 10c and 10d) and wavelet transform (Figures 10e and 10f) were applied.

[39] In detail, Figures 10c and 10d represent power spectra and statistical significance computed according to the hypothesis of background red noise. In both cases, peaks above the green dashed line (95% confidence spectrum) were assumed reliable. The first time series (Figure 10c) exhibits a major peak at ~11 min, while the second (Figure 10d) shows significant periods between ~7 and 14 min. This is consistent with the WT results (Figures 10e and 10f), which show significant spectral power (highlighted by the solid contour at 95% confidence interval) around 800 s for the upwelling zone and 200–800 s for the lake center. It is noteworthy that the peaks with frequency higher than 0.003 Hz (peaks overcoming the green dashed line, not included within the dashed black square in both Figures 10e and 10f) were neglected as they were characterized by low power values. The time series are unfortunately quite short and the edge effect is significant as evident from the cone of influence shown in Figures 10e and 10f.

6. Discussion

[40] Although the thermal survey was of a limited duration, the results still yield valuable insights into the lake activity, especially considering the inaccessibility of this volcano and the poor record of observations collected directly from the field. The lake upwelled along its southern margin, as observed at least from 2001 to 2005 [*Oppenheimer and Yirgu*, 2002; *Burgi et al.*, 2002; *Oppenheimer et al.*, 2004; *Harris et al.*, 2005; *Sawyer et al.*, 2008b], confirming a somewhat stable mode of convection despite reported fluctuations in lava lake height. This was 73, 80, 100, 45, and 53 m below the crater rim in February 2001, February 2002, March 2003, October 2005, and November 2006, respectively [*Oppenheimer and Yirgu*, 2002; *Oppenheimer et al.*, 2004; *Harris et al.*, 2005; *Sawyer et al.*, 2008b]. While the stable mode of convection reflects steady circulation (magma recycling) between the lake and the underlying reservoir, variations in magma level within the crater are related to magma pressures in the connected reservoir [*Oppenheimer and Francis*, 1997], thus to changes in the magma supply rate [*Oppenheimer et al.*, 2004].

[41] The lake displayed moderate activity in between the sluggish and vigorous convective regimes described by *Harris et al.* [2005] corresponding to variations of lake surface speeds from 0.01 to 0.15 m s^{-1}, consistent with estimates by *Harris et al.* [2005]. Peaks in brightness temperature (~1070°C) are comparable with those measured during previous direct and remote sensing surveys [*Barberi et al.*, 1973; *Allard et al.*, 1977; *Le Guern et*

al., 1979; *Burgi et al.*, 2002; *Oppenheimer and Yirgu*, 2002; *Oppenheimer et al.*, 2004; *Harris et al.*, 2005]. The frequency spatial distribution of temperatures varied according to the dynamics of the lake surface, specifically as the proportions of crust and exposed molten lava varied. Mean temperatures were approximately constant between ~400 and ~500°C, whereas maximum apparent temperatures showed greater variability.

[42] Radiant heat power outputs (Q_{rad}) estimated for the entire lake surface ranged from ~45 to 76 MW (taking the lake area of ~2500 m^2), in between ~70–150 MW estimated by *Oppenheimer and Yirgu* [2002] with a lake total area of 6200 m^2 and 5–30 MW calculated by *Oppenheimer et al.* [2004] with a lake surface of 910 m^2. This radiative power is dominated by the crust of the lava lake, and changes in the mean lake temperature therefore are reflected in Q_{rad}. The oscillations in radiative power can be explained by cycles of lake recharge, in which the influx of gas-rich, hot magma into the lake triggers lake inflation (a small increase in the lava level) promoting crust cracking and crack widening, opening of hot spots, lava and gas output from hot spots, and increased overturning and resurfacing rate. These variations may be associated with the dynamics of bubbly flow in the conduit as suggested by experimental observations of *Witham et al.* [2006], which these authors linked to changes in lake level. Lava lake cyclicity has been reported at other volcanoes, including Kilauea, Hawaii, where *Flynn et al.* [1993] identified variability of the thermal output of Kupaianaha lava lake on timescales of seconds to minutes.

[43] Figures 10a and 10b suggest two kinds of signals in the radiation power time series: high-frequency and high-amplitude variations and pulsing described by lower-frequency cycles. For each of the two time series, integrating information on the behavior of signal, the activity observed at the lake surface, and lava lake surface speeds, allowed us to infer the passages from high- to low-frequency dominated cycles to the transition from the vigorous to sluggish regimes described by *Harris et al.* [2005]. The high frequencies characterizing the first half of Figure 10b appear correlated with gas emissions from hot spot activity (vigorous activity). In the second half of the time series there is a transition to sluggish regime, associated with decrease in hot spot event frequency. The time series shown by Figure 10a behaves differently displaying a more regular trend marked by three dominant fluctuations. This is probably because it represents the vent area, whereas data from Figure 10b were recorded at the center of the lake where the surface activity was more dynamic and crust cracking, hot spot opening, and explosive activity occurred more frequently resulting in a noisier signal.

[44] Time series analysis carried out on radiant power measurements indicates two main periods of 11 min for the upwelling zone and 7–14 min for the lake center. These cycles could be associated with four main features: (1) incandescent cracks passing through the camera's field of view, (2) hot spot occurrence, (3) degassing cycles, and (4) crack widening due to lake inflation (arising from magma influx) or an increased overturning rate producing crust dilatation. However, *Harris et al.* [2005] found that incandescent crack activity is related to higher-frequency signals in thermal energy up to 0.04 Hz (25 s period) than our periods ranging between ~10 and 14 min (lower frequencies).

[45] From our observations, we suggest the cycles relate to the occurrence and activity of intraplate hot spots [*Harris et al.*, 2005] in both the vent area and the lake center, producing increases of incandescent areas exposed by hot gas emissions, and crust assimilation (features related to hot spot opening). *Harris* [2008] concluded that vigorous convection with high surface velocities results from the arrival at the surface of hot, crystal-poor lava. Integrating the surface speeds we estimated, we suggest that the observed periodicities are related to the rates of gas bubbles arriving at the surface, derived from new magma batches feeding the lake from a shallow reservoir. This is also consistent with the small increase of the lake level occurring during the vigorous activity and the hot spot opening, probably resulting from stages of gas-piston actions (gas cycles) as suggested by *Tilling* [1987].

[46] According to the experimental model of *Witham et al.* [2006] the cyclic activity of lava lakes, governed by the convection dynamics, can be divided into three main phases: (1) a recharge phase, where the upward flux of new less dense magma from the shallow reservoir fills the lake; (2) growth and separation of gas bubbles from the rising magma body and release of slugs of gas at the lake surface; (3) increase in the lake maximum depth with increase in magmastatic pressure at the base of the conduit and inhibition of the magma upflow within the lake and drainage along the downwelling edge. When a sufficient volume of magma has drained back through the feeding conduit,

the mechanism resumes with the recharge phase and bubbles rising back again up into the conduit.

[47] On 11 November 2006, the detected transition from vigorous activity with hot spot opening, rising of the lake level and high rates of magma convection, to the sluggish stage could represent the passage from the second to the third phase of the convective cycle described by *Witham et al.* [2006], with the second phase characterized by ~10–14 min period.

7. Concluding Remarks

[48] Thermal imaging performed on the active lava lake of Erta 'Ale volcano on 11 November 2006 provided valuable information on the lake's eruptive state. Thermal image analysis allowed us to examine the lava lake convective stability and to identify transitions of the eruptive regime from vigorous to sluggish phases. These were reflected in variations of lava convection lake surface speed, mean temperatures, and radiant power output from the lake surface. Time series analysis carried out on the measured radiant power output highlighted low-amplitude periods (11 min for the upwelling zone and 7–14 min for the center of the lake) related to the regular release of overpressured gas bubbles. Our data set was obtained opportunistically and longer data sets are necessary to explore further the cyclic behavior of the lake in terms of magma supply and degassing, especially in respect of identifying low-frequency signals.

Acknowledgments

[49] We wish to thank G. Di Grazia and S. Falsaperla from INGV Catania Section and C. Keylock from the University of Leeds for their helpful suggestions in time series processing. LS is grateful to GM Sawyer for sharing Erta 'Ale information. LS acknowledges a Ph.D. grant funded by the project "Sviluppo di sistemi di monitoraggio" (Dipartimento di Protezione Civile di Regione Sicilia, INGV Catania Section, Italy). CO thanks the Leverhulme Trust for a Study Abroad Fellowship and the BBC along with Iain Stewart, Jonathan Renouf, Paul Olding, Elizabeth Vancura, Tim Cragg, Adam Prescod, and the Ethiopian Air Force for support of the expedition to Erta 'Ale.

References

Allard, P., F. Le Guern, and J. C. Sabroux (1977), Thermodynamics and isotopic studies in eruptive gases, *Geothermics*, *5*, 37–40, doi:10.1016/0375-6505(77)90006-2.

Allard, P., C. Oppenheimer, A. J. S. McGonigle, A. Aiuppa, M. F. Le Cloarec, M. J. Wooster, and V. Tsanev (2004), Magma supply rate to Erta 'Ale lava lake (Afar) inferred from measured volatile and heat fluxes, *Geophys. Res. Abstr.*, *6*, 06601, Sref-ID:1607–7962/gra/EGU04-A-06601.

Ball, M., and H. Pinkerton (2006), Factors affecting the accuracy of thermal imaging cameras in volcanology, *J. Geophys. Res.*, *111*, B11203, doi:10.1029/2005JB003829.

Barberi, F., J. L. Cheminée, and J. Varet (1973), Long-lived lava lakes of Erta 'Ale volcano, *Rev. Geogr. Phys. Geol. Dyn.*, *15*, 347–351.

Bartosch, T., and D. Seidl (1999), Spectrogram analysis of selected tremor signals using short-time Fourier transform and continuous wavelet transform, *Ann. Geofis.*, *42*(3), 497–506.

Burgi, P. Y., M. Caillet, and S. Haefeli (2002), Field temperature measurements at Erta 'Ale Lava Lake, Ethiopia, *Bull. Volcanol.*, *64*, 472–485, doi:10.1007/s00445-002-0224-3.

Calkins, J., C. Oppenheimer, and P. R. Kyle (2008), Ground-based thermal imaging of phonolite lava lakes at Erebus volcano, Antarctica, *J. Volcanol. Geotherm. Res.*, doi:10.1016/j.volgeores.2008.02.002, in press.

Daubechies, I. (1990), The wavelet transform time frequency localization and signal analysis, *IEEE Trans. Inf. Theory*, *36*, 961–1004, doi:10.1109/18.57199.

Flynn, L. P., P. J. Mouginis-Mark, J. C. Gradie, and P. G. Lucey (1993), Radiative temperature measurements at Kupaianaha lava lake, Kilauea Volcano, Hawaii, *J. Geophys. Res.*, *98*(B4), 6461–6476, doi:10.1029/92JB02698.

Francis, P. W., C. Oppenheimer, and D. Stevenson (1993), Endogenous growth of persistently active volcanoes, *Nature*, *366*, 554–557, doi:10.1038/366554a0.

Global Volcanism Network (1992), Erta 'Ale, *Global Volcanism Network Bull.*, *17*, 11.

Grinsted, A., J. C. Moore, and S. Jevrejeva (2004), Application of the cross wavelet transform and wavelet coherence to geophysical time series, *Nonlinear Proc. Geophys.*, *11*, 561–566.

Harris, A. J. L. (2008), Modeling lava lake heat loss, rheology, and convection, *Geophys. Res. Lett.*, *35*, L07303, doi:10.1029/2008GL033190.

Harris, A. J. L., L. Flynn, D. A. Rothery, C. Oppenheimer, and S. B. Sherman (1999), Mass flux measurements at active lava lakes: Implications for magma recycling, *J. Geophys. Res.*, *104*, 7117–7136, doi:10.1029/98JB02731.

Harris, A. J. L., R. Carniel, and J. Jones (2005), Identification of variable convective regimes at Erta 'Ale lava lake, *J. Volcanol. Geotherm. Res.*, *142*, 207–223, doi:10.1016/j.jvolgeores.2004.11.011.

Hildebrandt, J. M. (1875), Erlebnisse auf einer Reise von Massûa in das Gebiet der Afer und nach Aden, *Z. Ges. Erdkunde Berlin*, *10*, 1–38.

Howell, R. R., and R. M. C. Lopes (2007), The nature of the volcanic activity at Loki: Insights from Galileo NIMS and PPR data, *Icarus*, *186*, 448–461, doi:10.1016/j.icarus.2006.09.022.

Huppert, H. E., and M. A. Hallworth (2007), Bi-directional flows in constrained systems, *J. Fluid Mech.*, *578*, 95–112, doi:10.1017/S0022112007004661.

Jones, J., R. Carniel, A. J. L. Harris, and S. Malone (2006), Seismic characteristics of variables convection at Erta 'Ale lava lake, Ethiopia, *J. Volcanol. Geotherm. Res.*, *153*, 64–79, doi:10.1016/j.jvolgeores.2005.08.004.

Karlstrom, L., and M. Manga (2006), Origins and implications of zigzag rift patterns on lava lakes, *J. Volcanol. Geotherm. Res.*, *154*, 317–324, doi:10.1016/j.jvolgeores.2006.01.004.

Kazahaya, K., H. Shinohara, and G. Saito (1994), Excessive degassing of Izu-Oshima volcano: Magma convection in a conduit, *Bull. Volcanol.*, *56*, 207–216, doi:10.1007/BF00279605.

Le Guern, F., J. Carbonelle, and H. Tazieff (1979), Erta 'Ale lava lake: Heat and gas transfer to the atmosphere, *J. Volcanol. Geotherm. Res.*, *6*, 27–48, doi:10.1016/0377-0273(79)90045-3.

Lesage, P., F. Glangeaud, and J. Mars (2002), Applications of autoregressive and time-frequency analysis to the study of volcanic tremor and LP events, *J. Volcanol. Geotherm. Res.*, *114*, 391–417, doi:10.1016/S0377-0273(01)00298-0.

Matson, D. L., A. G. Davies, G. J. Veeder, J. A. Rathbun, T. V. Johnson, and J. C. Castillo (2006), Io: Loki Patera as a magma sea, *J. Geophys. Res.*, *111*, E09002, doi:10.1029/2006JE002703.

Munzinger, W. (1869), Narrative of a journey through the Afar country, *J. R. Geogr. Soc.*, *39*, 188–232.

Oppenheimer, C., and P. Francis (1997), Remote sensing of heat, lava and fumarole emissions from Erta 'Ale volcano, Ethiopia, *Int. J. Remote Sens.*, *18*(8), 1661–1692, doi:10.1080/014311697218043.

Oppenheimer, C., and P. Francis (1998), Implications of long-eval lava lakes for geomorphological and plutonic processes at Erta 'Ale volcano, Afar, *J. Volcanol. Geotherm. Res.*, *80*, 101–111, doi:10.1016/S0377-0273(97)00041-3.

Oppenheimer, C., and G. Yirgu (2002), Thermal imaging of an active lava lake: Erta 'Ale volcano, Ethiopia, *Int. J. Remote Sens.*, *23*, 4777–4782, doi:10.1080/01431160110114637.

Oppenheimer, C., A. J. S. McGonigle, P. Allard, M. J. Wooster, and V. Tsanev (2004), Sulphur, heat, and magma budget of Erta 'Ale lava lake, Ethiopia, *Geology*, *32*, 509–512, doi:10.1130/G20281.1.

Sawyer, G. M., S. A. Carn, V. I. Tsanev, C. Oppenheimer, and M. Burton (2008a), Investigation into magma degassing at Nyragongo volcano, Democratic Republic of Congo, *Geochem. Geophys. Geosyst.*, *9*, Q02017, doi:10.1029/2007GC001829.

Sawyer, G. M., C. Oppenheimer, V. Tsanev, and G. Yirgu (2008b), Magmatic degassing at Erta 'Ale volcano, Ethiopia, *J. Volcanol. Geotherm. Res.*, in press.

Stevenson, D. S., and S. Blake (1998), Modelling the dynamics and thermodynamics of volcanic degassing, *Bull. Volcanol.*, *60*, 307–317, doi:10.1007/s004450050234.

Sweeney, D., P. R. Kyle, and C. Oppenheimer (2008), Sulphur dioxide emissions and degassing behaviour of Erebus volcano, Antarctica, *J. Volcanol. Geotherm. Res.*, doi:10.1016/j.jvolgeores.2008.01.024, in press.

Tazieff, H. (1973), The Erta 'Ale volcano, *Rev. Geogr. Phys. Geol. Dyn.*, *15*, 437–441.

Tazieff, H. (1994), Permanent lava lakes - Observed facts and induced mechanisms, *J. Volcanol. Geotherm. Res.*, *63*, 3–11, doi:10.1016/0377-0273(94)90015-9.

Thesiger, W. (1996), *The Danakil Diary: Journeys Through Abyssinia/Wilfred Thesiger, 1930–34*, Harper Collins, London.

Tilling, R. I. (1987), Fluctuations in surface height of active lava lakes during 1972–1974 Mauna Ulu eruption, Kilauea volcano, Hawaii, *J. Geophys. Res.*, *92*, 13,721–13,730, doi:10.1029/JB092iB13p13721.

Torrence, C., and G. P. Compo (1998), A practical guide to wavelet analysis, *Bull. Am. Meteorol. Soc.*, *79*, 61–78, doi:10.1175/1520-0477(1998)079<0061:APGTWA>2.0.CO;2.

Turcotte, D. L., and G. Schubert (2002), Fluid mechanics, in *Geodynamics*, pp. 226–291, Cambridge Univ. Press, New York.

Witham, F., and E. W. Llewellin (2006), Stability of lava lakes, *J. Volcanol. Geotherm. Res.*, *158*, 321–332, doi:10.1016/j.jvolgeores.2006.07.004.

Witham, F., A. W. Woods, and C. Gladstone (2006), An analogue experimental model of depth fluctuations in lava lakes, *Bull. Volcanol.*, *69*, 51–56, doi:10.1007/s00445-006-0055-8.